Analysis of the performance of a particle velocity sensor between two cylindrical obstructions

J. W. van Honschoten,[a] D. R. Yntema, V. B. Svetovoy, M. Dijkstra, R. J. Wiegerink, and M. Elwenspoek

Transducers Science and Technology Group, MESA+ Institute for Nanotechnology, University of Twente, The Netherlands

(Received 19 May 2006; revised 20 February 2007; accepted 22 February 2007)

The performance of an acoustic particle velocity sensor that is placed between two cylindrical objects has been analyzed both analytically and by means of finite volume simulations on fluid dynamics. The results are compared with acoustic experiments that show a large magnification of the output signal of the particle velocity sensor due to the mounting of the sensor between two cylinders. The influences of this construction consist of an attenuation of particle velocities at frequencies below a few hertz, whereas signals in the higher frequency range are amplified, up to approximately three times (10 dB) in a frequency range between 50 and 1000 Hz. The theoretical analysis is based on the derivation of the stream function for the situation of two long cylinders immersed in an oscillating incompressible viscous fluid, at low Reynolds numbers. The results lead to an improved insight into the effects of viscosity and fluid flow that play a role in acoustic measurements and open the way for further optimization of the sensitivity of the sensor. © *2007 Acoustical Society of America.* [DOI: 10.1121/1.2717406]

PACS number(s): 43.58.Fm, 43.20.Ye [AJZ] Pages: 2711–2722

I. INTRODUCTION

This paper discusses a micromachined acoustic sensor based on a thermal measurement principle that measures particle velocity instead of sound pressure, the scalar quantity that is measured by conventional microphones.[1,2] The sensor has been optimized for sound measurement purposes, and it has been applied to the measurement of one- and three-dimensional sound intensities,[2] acoustic impedances,[3,4] and far field pressure.[5] Other applications of the sensor such as an add-on microphone for professional recording purposes have also been shown.[6] An important property of the particle velocity sensor, contrary to pressure gradient microphones, is its comparatively high sensitivity to low frequency sound waves; it can thus be used as well for the measurement of dc flows,[7] and it can be applied as a mass flow sensor.

A thermal particle velocity sensor usually consists of two closely spaced (spacing about 100 μm) thin wires of silicon nitride, with an electrically conducting platinum pattern on top of them, as shown in Fig. 1. The dimensions of the two wires are $1500\times2\times0.3$ μm. The platinum layer on top of the silicon nitride is used as a heater *and* as a temperature sensor by using the temperature-dependent resistance of the platinum. The wires are heated by an electrical current to an operation temperature between 300 and 400 °C. The particle velocity associated with the sound wave will modulate the temperature distribution around the resistors, which can be measured electronically due to the related change in resistance values.

In 2000, a theoretical description and a model for the behavior of the device were presented[8] and an explicit analytical expression for the sensitivity was deduced.[9,10]

For measurement purposes, the particle velocity sensor is placed in a protective package: an approximately 7-cm-long cylindrical probe of 13 mm diameter with two small cylinders of 5 mm diameter at its end, with the sensor in between [see Fig. 2 for a picture of the commercially available "PU" probe and Figs. 3(b) and 3(c) for a model representation]. This packaging of the sensor improves its sensitivity considerably. In the case of our experimental device the sensitivity was increased by a factor of 3.2, or approximately 10 dB at 500 Hz. This observation raised the need for a detailed investigation of the effects of the two adjoining cylindrical objects of the package, in order to optimize the sensor performance further. In this paper, this investigation is achieved both by a theoretical description of the flow profile around two long cylinders and by a numerical analysis by means of finite-volume computational fluid dynamic simulations on this two cylinder geometry and on the specific probe package with its two small cylindrical tubes.

The phenomenon of oscillatory viscous flow around a long cylinder has been subject of investigation for many years, especially for high Reynolds numbers. One of the points of interest has been the time-independent streaming motion as a result of the interaction of the oscillatory viscous flow with a solid boundary. This induced steady streaming is generated by the nonlinear Reynold stresses in the unsteady boundary layer. For Reynolds numbers $\mathrm{Re}\sim10$ the steady streaming near an oscillating circular cylinder was studied by Carrière,[11] while Andrade[12] and Schlichting[13] did experiments in the range $\mathrm{Re}\sim1000$. A theory in terms of expansions in the inner and outer regions around the cylinder was proposed by Riley.[14] Wang[15] solved the problem of oscillatory viscous flows around a single cylinder, for a broad range of Reynolds and Strouhal numbers. Zapranov *et al.*[16] ana-

[a]Electronic mail: j.w.vanhonschoten@utwente.nl

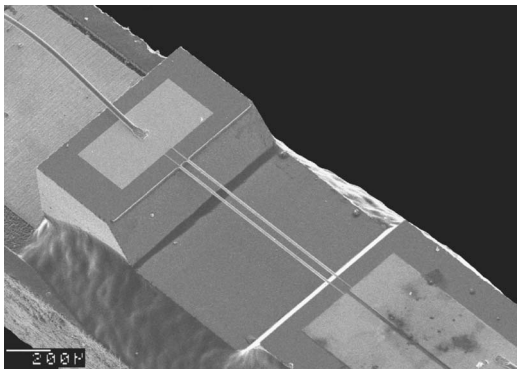

FIG. 1. SEM photograph of a two-wire type particle velocity sensor.

lyzed the flow around two parallel cylinders with the plane of their axes both perpendicular and parallel to the flow, whereas they concentrated on the high Reynolds number range when steady streaming becomes important. Flow around two parallel cylinders placed one behind the other in the propagation of an acoustic sound wave was studied by Zhuk *et al.*[17] Two parallel cylinders in an oscillatory flow have also been investigated numerically,[18] but especially for relatively high Reynolds numbers (Re$\sim$200).

In this paper, however, we concentrate on the oscillatory flow due to a sound wave around two parallel cylinders in the range of low Reynolds numbers (Re$\sim$1) since the typical velocities associated with sound waves are relatively small. The equations to be solved then become linear.[19] We follow broadly the approach proposed by Zapryanov *et al.*,[16] but investigate especially the fluid flow for small particle velocities. The assumption that we shall make is that the characteristic dimensions of the problem ($\sim$15 mm) are much smaller than the acoustic wavelength, which is valid for frequencies much lower than 20 kHz. In this case the propagation of interactions in the gas can be regarded as instantaneous, which, together with the condition that the fluid velocity be small compared with that of sound, implies that the fluid can be described as incompressible.

FIG. 2. The commercially available PU probe, with the particle velocity sensor packaged in between the two cylinders.

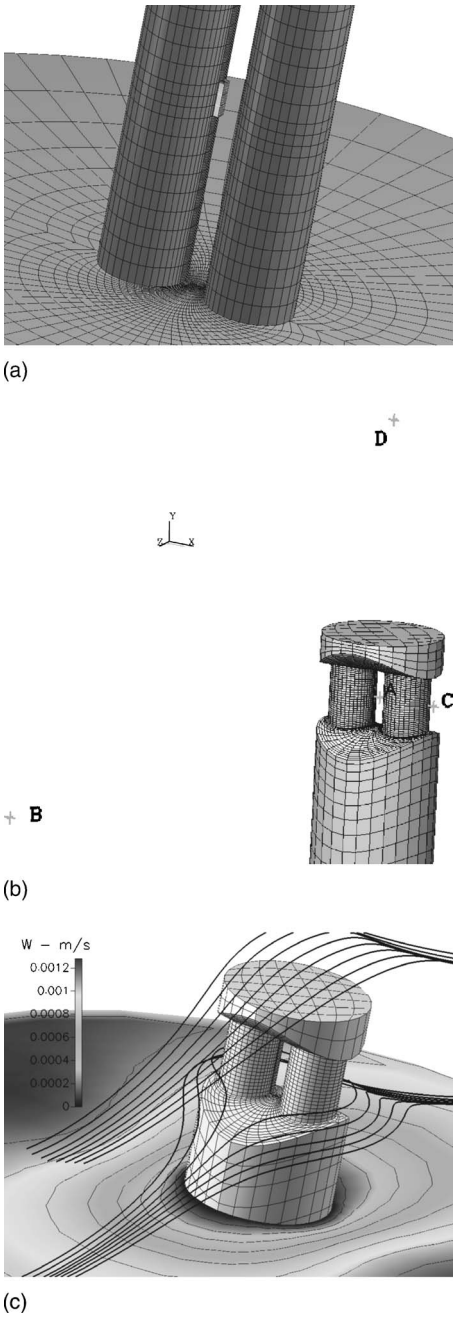

FIG. 3. (a) The solution space for numerical calculations on two long cylinders with a small rectangular obstacle at fixed temperature in between. The geometry consists of 50 000 cells. (b) A grid containing about 70 000 cells is defined to model the probe geometry, very dense structured at the place of interest (the center). Four points in space were defined in particular: point *A*: in between the two cylinders, *B*: at large distance in front of the probe, *C*: left from the probe, 6.5 mm from the center, *D*: at 3 cm above *A*. (c) Simulation result visualizing both the instantaneous streamlines (defined at a particular time $t=t_0$) and a contour plot of the particle velocity at $v_0=1$ mm/s; $f=1$ Hz.

II. THEORY

A. Introduction

For a description of the flow behavior around the sensor, the full Navier-Stokes equations for the three-dimensional geometry should be solved. For the complex geometry of the actual probe as shown in Fig. 2, an exact solution cannot be found.

However, the two cylindrical obstructions of this package on both sides of the particle velocity sensor raise the need for an analysis of the acoustic flow profile around two parallel long cylinders, a problem that is actually two dimensional. As will be shown in the following, the solution to this two-dimensional problem offers a quite adequate description of the more complicated probe geometry.

B. Assumptions and problem definition

To find the flow profile in and around the geometry of interest, we have to solve the equations of motion of a viscous fluid, the Navier-Stokes equations. In their most general form, these equations are rarely solvable for complicated geometries. Therefore, several assumptions to simplify the problem and some approximations have to be made.

In the following approach the influence of the sensor between the two cylinders on the flow behavior will be neglected, and the fluid is considered as incompressible. In that case the problem consists of a viscous fluid of constant density ρ and kinematic viscosity ν in which two separated parallel cylinders are immersed. At infinity, the fluid oscillates harmonically, perpendicular to the plane containing their axes, with a velocity $u_0 \cos \omega t$. Two regions of interest are distinguished: a frequency range $\omega \ll \omega_c$, in which viscous effects will be seen to be dominant and the viscous boundary layers around the cylinders become large, and a region $\omega \gg \omega_c$, where the fluid behavior approaches that of an ideal gas.

To determine if the fluid in the case of propagating acoustic waves can be regarded as incompressible, we consider the conditions under which the assumption of incompressibility is justified. The fluid may be regarded as incompressible if $\Delta\rho/\rho \ll 1$. A necessary condition for this is that the fluid velocity be small compared with that of sound:[20]

$$v \ll c. \tag{1}$$

However, this condition is sufficient only in steady flow. In nonsteady flow, a further condition must be fulfilled. If τ is a characteristic time over which the fluid velocity undergoes significant changes, then the second condition reads

$$\tau \gg l/c. \tag{2}$$

Condition (2) means in fact that the time l/c taken by a sound signal to traverse the distance l must be small compared with the time τ during which the flow changes appreciably, so that the propagation of interactions in the gas may be regarded as instantaneous. The characteristic length l of the problem is orders of magnitude smaller than the acoustic wave length.

Typical values for the magnitude of the particle velocity of sound waves are $v = 10^{-5} - 10^{-2}$ m s^{-1}. Taking $v = 2.5 \times 10^{-3}$ m s^{-1} ($\sim$94 dB sound level), $c = 350$ m s^{-1}, $l = 5$ mm, we see that for all frequencies well below 10 kHz, conditions (1) and (2) are fulfilled, and one can describe the gas as incompressible.

In their most general form the Navier-Stokes equations for an incompressible fluid then read

$$\frac{\partial \mathbf{v}}{\partial t} + (\mathbf{v} \cdot \boldsymbol{\nabla})\mathbf{v} = -\frac{1}{\rho} \boldsymbol{\nabla} p + \nu \nabla^2 \mathbf{v} \tag{3}$$

with $\mathbf{v}$ the (vectorial) velocity, p the pressure, ν the kinematic viscosity, and ρ the fluid density.

Besides, the continuity equation has to be obeyed:

$$\frac{\partial \rho}{\partial t} + \rho \boldsymbol{\nabla} \cdot \mathbf{v} = 0. \tag{4}$$

Let us assume an infinite incompressible viscous fluid in which two parallel circular cylinders of radius R are immersed. The presence of the sensor itself and its high temperature are neglected as yet, later we will see the justification for this. The fluid oscillates in the direction perpendicular to the plane containing the axes of the cylinders with velocity $u_0 \cos 2\pi f t$ at infinity where u_0 is the magnitude of the particle velocity and f the frequency of the wave.

The problem is scaled using the dimensionless parameters

$$\tau = \frac{\nu}{l^2} t, \quad \mu = \frac{2\pi f l^2}{\nu}, \tag{5}$$

where l represents a characteristic length, e.g., the cylinder radius.

The Navier-Stokes equations in the form (3) are nonlinear because of the second term on the left-hand side. This nonlinear problem has been analyzed by Zapryanov *et al.*[16] They used a perturbation theory in terms of asymptotic expansions in the inner and outer regions around the cylinders.[15,16]

We can estimate the nonlinear convection term $(\mathbf{v} \cdot \boldsymbol{\nabla})\mathbf{v}$ to be in the order of u_0^2/l, while the magnitude of the time-dependent term can be approximated as ωu_0 and the viscous term as $\nu u_0/l^2$. One sees that the nonlinear term can be neglected compared with the other terms in the Navier-Stokes equations if

$$u_0 \ll \max\left\{\frac{\nu}{l}, 2\pi f l\right\}. \tag{6}$$

For the current values in our problem, $u_0 \sim 2 \times 10^{-4}$ m/s, $l \sim 6 \times 10^{-3}$ m, and $\nu \sim 1.5 \times 10^{-5}$ m^2/s, corresponding to a Reynolds number of $\mathrm{Re} \ll 1$. Taking as a lower limit for the frequency 1 Hz, we see that $\nu/l \approx 3 \times 10^{-3}$ m/s and $2\pi f l \approx 4 \times 10^{-2}$ m/s so that condition (6) is well fulfilled.

Further, we assume $\mu \gg 1$.

Taking the curl of both sides of Eq. (3) and using the equation $\boldsymbol{\nabla} \cdot \mathbf{v} = 0$, we get

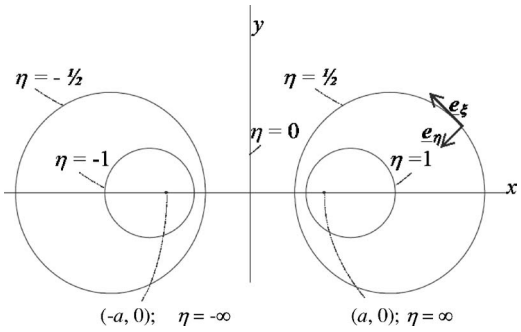

FIG. 4. Representation of the used coordinate system.

$$\frac{\partial}{\partial \tau}(\nabla \times \mathbf{v}) + (\mathbf{v} \cdot \nabla)\, \nabla \times \mathbf{v} - (\nabla \times \mathbf{v} \cdot \nabla)v = \frac{1}{\mu}\Delta(\nabla \times \mathbf{v}). \tag{7}$$

The equations of motion, Eq. (3), are often written in terms of the stream function Ψ,[16,20] defined by

$$\nu_x = \frac{\partial \Psi}{\partial y}, \quad \nu_y = -\frac{\partial \Psi}{\partial x}. \tag{8}$$

Neglecting now the nonlinear terms, one obtains with Eqs. (7) and (8) the equation to be solved for the stream function

$$\frac{\partial}{\partial \tau}(\Delta \Psi) - \frac{1}{\mu}\Delta^2 \Psi = 0. \tag{9}$$

C. Solution

The problem can be well described in a two-dimensional system of bipolar cylindrical coordinates (ξ, η), defined by the transformations

$$x = \frac{a \sinh \eta}{\cosh \eta - \cos \xi}, \quad y = \frac{a \sin \xi}{\cosh \eta - \cos \xi}, \quad a = 1, \tag{10}$$

where x and y are the usual Cartesian coordinates, $0 \leqslant \xi < 2\pi$ and $-\infty < \eta < \infty$. See Fig. 4. The value of the length parameter a is in principle arbitrary, for convenience we have chosen it as yet to be $a=1$. The two cylinders are therefore defined by $\eta = \eta_1 > 0$ and $\eta = \eta_2 < 0$, such that $R = a/|\sinh \eta_1| = a/|\sinh \eta_2|$ and we consider the symmetric case $\eta_1 = -\eta_2$. The fluid region is given by $\eta_2 < \eta < \eta_1$, $0 \leqslant \xi < 2\pi$, while $\eta = \xi = 0$ at infinity.

In this coordinate system, the stream function Ψ is defined by

$$\nu_\xi = (\cosh \eta - \cos \xi)\frac{\partial \Psi}{\partial \eta}, \quad \nu_\eta = -(\cosh \eta - \cos \xi)\frac{\partial \Psi}{\partial \xi}. \tag{11}$$

The equation for the stream function,

$$\frac{\partial}{\partial \tau}(\Delta \Psi) - \frac{1}{\mu}\Delta^2 \Psi = 0, \tag{12}$$

is to be solved in the (ξ, η) plane, with Δ the Laplacian operator in this coordinate system, i.e.,

$$\Delta = (\cosh \eta - \cos \xi)^2 \left(\frac{\partial^2}{\partial \xi^2} + \frac{\partial^2}{\partial \eta^2} \right). \tag{13}$$

If $\psi_1 - \psi_2$ is the (dimensionless) total flux between the two cylinders, the boundary conditions for Ψ become

$$\Psi = \psi_i, \quad \frac{\partial \Psi}{\partial \eta} = 0 \quad \text{at } \eta = \eta_i \quad (i = 1,2), \tag{14}$$

$$\Psi = \frac{-\sinh \eta}{\cosh \eta - \cos \xi} e^{i\tau} \quad \text{at } \eta \to 0, \quad \xi \to 0. \tag{15}$$

We assume an oscillatory flow with time dependence $e^{i\tau}$, $\tau = 2\pi f t$, and eliminate this time dependence in the equations by defining $\Psi = \bar{\Psi}(\xi, \eta, \tau)e^{i\tau}$. This results in

$$\frac{\partial}{\partial \tau}(\Delta \bar{\Psi}) + i\Delta \bar{\Psi} - \frac{1}{\mu}\Delta^2 \bar{\Psi} = 0. \tag{16}$$

For convenience, the bar on Ψ is omitted from now on, and after neglecting the slow time dependence, the equation to be solved becomes

$$\Delta(\Delta \Psi - i\mu \Psi) = 0. \tag{17}$$

To do this, we divide the fluid region into separate regions: two thin boundary layers around both cylinders, and an intermediate region outside these layers. Besides, the problem is symmetric in the axis $\eta = 0$ (we consider the case $\eta_1 = \eta_2$), so we restrict ourselves to the region $\eta > 0$ (with only one cylinder and one boundary layer) and realize that the final stream function is an antisymmetric function in η.

In the region outside the boundary layer, we can neglect viscous effects and make use of the assumption that μ is large, so that the equation for the stream function to be solved reduces to the Laplace equation:

$$\Delta \Psi = 0 \tag{18}$$

including the boundary conditions (14) and (15).

With the following coordinate transformation to p and q:

$$p = \frac{\xi + i\eta}{2}, \quad q = \frac{\xi - i\eta}{2} \tag{19}$$

so that $(\cosh \eta - \cos \xi) = 2 \sin p \sin q$, the Laplace equation in p, q coordinates reads

$$\sin^2 p \sin^2 q \frac{\partial^2}{\partial p \partial q}\Psi = 0 \tag{20}$$

we see that every function of the form $\Psi(p,q) = f_1(p) + f_2(q)$ is a solution, where f_1 and f_2 are functions that depend only on p and only on q, respectively. Since the boundary condition (15) can be written as $\Psi = -(i/2)(\cot p - \cot q)$ for $p \to 0, q \to 0$, the stream function

$$\Psi = -\frac{i}{2}\left(\cot \frac{\xi + i\eta}{2} - \cot \frac{\xi - i\eta}{2} \right) = \frac{-\sinh \eta}{\cosh \eta - \cos \xi} \tag{21}$$

obeys the Laplace equation, Eq. (18), and condition (15). To meet the other boundary condition, Eq. (14), we add two functions $f_1(p)$ and $f_2(q)$, that have to be determined from the requirement:

$$\Psi = \Psi_0 \quad \text{at } \eta = \eta_1 \tag{22}$$

with Ψ_0 a constant. Besides, Ψ is 2π periodic in ξ.

Writing f_1 and f_2 in the form of expansions,

$$f_1\left(\frac{\xi + i\eta}{2}\right) = \sum_{n=-\infty}^{\infty} a_n \exp\left(2in\frac{\xi + i\eta}{2}\right),$$

$$f_2\left(\frac{\xi - i\eta}{2}\right) = \sum_{n=-\infty}^{\infty} b_n \exp\left(2in\frac{\xi - i\eta}{2}\right), \tag{23}$$

the sum of them, $f_1((\xi+i\eta)/2)+f_2((\xi-i\eta)/2)$, can be written in the form

$$\sum_{n=-\infty}^{\infty} (a_n e^{-n\eta} + b_n e^{n\eta}) e^{in\xi}. \tag{24}$$

This infinite series should converge for all $0 \leqslant \eta \leqslant \eta_1$, $0 \leqslant \xi \leqslant 2\pi$ and moreover, the final function has to be even in ξ. These requirements lead to the following expression for the series:

$$f_1\left(\frac{\xi + i\eta}{2}\right) + f_2\left(\frac{\xi - i\eta}{2}\right) = A_0 + \sum_{n=0}^{\infty} A_n e^{n\eta} \cos n\xi, \tag{25}$$

where the coefficients A_n follow from the boundary conditions at $\eta = \eta_1$:

$$A_n = \frac{\exp(-n\eta_1)}{\pi} \int_{-\pi}^{\pi} \left(\frac{\sinh \eta_1}{\cosh \eta_1 - \cos \xi}\right) \cos n\xi d\xi \tag{26}$$

The coefficients A_n, as expressed by Eq. (26) can be calculated explicitly[21] and become finally very simple:

$$A_n = 2 \exp(-2n\eta_1). \tag{27}$$

We thus find for the total stream function (that is defined up to an arbitrary constant) in the region outside the boundary layers:

$$\Psi(\xi, \eta) = \left(-\frac{\sinh \eta}{\cosh \eta - \cos \xi} + \sum_{n=1}^{\infty} A_n \exp(n\eta) \cos n\xi\right) \exp(i\tau) \tag{28}$$

with A_n as defined in Eq. (27).

With this expression for A_n the sum in Eq. (28) can be calculated straightforwardly and the stream function in the region outside the boundary layers becomes

$$\Psi(\xi, \eta) = \left(\frac{\exp(\eta - 2\eta_1 + i\xi)}{1 - \exp(\eta - 2\eta_1 + i\xi)} + \frac{\exp(\eta - 2\eta_1 - i\xi)}{1 - \exp(\eta - 2\eta_1 - i\xi)} - \frac{\sinh \eta}{\cosh \eta - \cos \xi}\right) \exp(i\tau). \tag{29}$$

Using the inverse transformation of Eq. (10), this can be written in Cartesian coordinates as

$$\Psi(x,y) = 2\,\mathrm{Re}\left(\left(\frac{y + i(x+a)}{y(\exp(2\eta_1) - 1) + i(x(\exp(2\eta_1 - 1)) - a(\exp(2\eta_1) + 1))}\right) - x\right) \exp(i\tau). \tag{30}$$

In the boundary layer adjacent to the right cylinder, Eq. (17) is solved by finding the solution of

$$\Delta \Psi_b - i\mu \Psi_b = 0 \tag{31}$$

with Ψ_b the stream function in this region and μ large but finite.

One can now introduce the scaled variable ζ in this region:

$$\zeta = (\eta_1 - \eta)\sqrt{\mu}. \tag{32}$$

The boundary layer extends from $\zeta = 0$ to $\zeta = 1$.

Since in this boundary layer η does not change significantly, and because the ξ derivatives of Ψ are small compared with the η derivatives, the equation to be solved becomes

$$\frac{\partial^2 \Psi_b}{\partial \zeta^2} - i(\cosh \eta_1 - \cos \xi)^2 \frac{\partial^4 \Psi_b}{\partial \zeta^4} = 0, \tag{33}$$

which has the solution

$$\Psi_b(\xi, \zeta) = C_1 \exp(\sqrt{i}(\cosh \eta_1 - \cos \xi)\zeta) + C_2 \exp(-\sqrt{i}(\cosh \eta_1 - \cos \xi)\zeta) + C_3\zeta + C_4. \tag{34}$$

The coefficients C_1, C_2, and C_3 are to be determined from the requirements for Ψ_b that

$$\Psi_b = \psi_1, \quad \frac{\partial \Psi_b}{\partial \zeta} = 0 \quad \text{at } \zeta = 0 \quad (\eta = \eta_1), \tag{35}$$

$$\frac{\partial \Psi_b}{\partial \zeta}\frac{d\zeta}{d\eta} = \frac{\partial \Psi}{\partial \eta} \quad \text{at } \zeta = 1 \quad (\eta = \eta_1 + 1/\sqrt{\mu}) \tag{36}$$

and, since the velocity v_ξ should also be continuous,

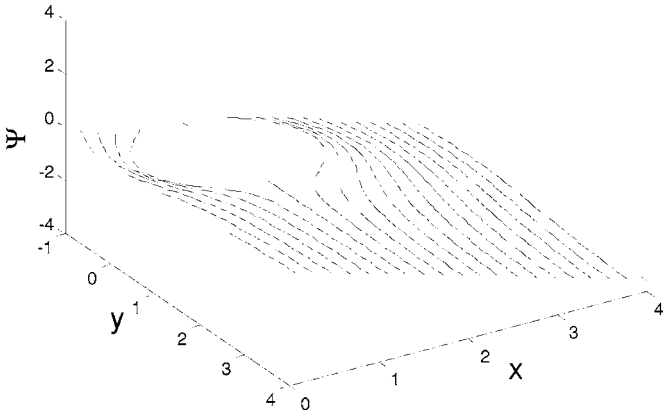

FIG. 5. Stream function Ψ as calculated from Eq. (29). Contour lines of Ψ form the streamlines in the flow.

$$M^2 \frac{\partial^2 \Psi_b}{\partial \zeta^2} = \frac{\partial^2 \Psi}{\partial \eta^2} \quad \text{at } \zeta = 1 \quad (\eta = \eta_1 + 1/\sqrt{\mu}). \tag{37}$$

Explicit expressions for the coefficients $C_1(\xi, \eta_1)$, $C_2(\xi, \eta_1)$, and $C_3(\xi, \eta_1)$ follow from a straightforward calculation from Eqs. (35), (36), and (37) but are not shown here for brevity. For a specific value of η_1 the result of Eq. (34) with these values of the coefficients is plotted in Fig. 6.

D. Discussion

The fluid region around the two cylinders has been divided in three regions: The two boundary layers adjacent to the cylinders, of thickness $\delta \sim R\mu^{-1/2}$, and a region in between. The Navier-Stokes equations are solved in terms of a stream function Ψ. In the boundary regions the stream function Ψ_b is governed by the parameter μ, and this solution is matched to the function Ψ in the intermediate region.

In Fig. 5, the stream function according to Eq. (29) is visualized in the x-y plane, for the half-infinite region $x > 0$ and a cylinder radius $R = \sinh \eta_1$ ($a = \eta_1 = 1$). Contour lines of Ψ form the streamlines of the flow.

Since the reduced frequency parameter $\mu = \pi f l^2 / \nu$ is proportional to frequency f, the situation $\mu \to \infty$ describes the nonviscous fluid limit, and the equation to be solved becomes the Laplace equation, Eq. (18). The ideal case of one infinitely long cylinder of radius R in an incompressible nonviscous ideal fluid with a velocity $u_0 e^{i2\pi ft}$ at infinity is relatively easily solved in radial coordinates, see, e.g., Landau.[20] As is also the case in our situation, this problem is two dimensional and it can be solved in terms of a potential function Φ and stream function Ψ (Φ and Ψ are the real and imaginary parts of the complex potential w, respectively). One then finds for the potential Φ and the velocity $\mathbf{v}$ of one cylinder immersed in a nonviscous fluid

$$\Phi = \frac{R^2}{r} \mathbf{u}_0 \cdot \mathbf{n} + \mathbf{u}_0 \cdot \mathbf{r}, \quad \mathbf{v} = \mathbf{u} - \frac{R^2}{r^2} (2\mathbf{n}(\mathbf{u}_0 \cdot \mathbf{n}) - \mathbf{u}_0) \tag{38}$$

with $\mathbf{n}$ a unit vector in the direction of $\mathbf{r}$ and with the origin as the center of the cylinder. We recognize in this expression the contribution of the uniform flow (the term $\mathbf{u}_0 \cdot \mathbf{r}$ in the expression for Φ), and a "doublet flow"[22] or "dipole" solution (the term $\mathbf{u}_0 \cdot \mathbf{n}/r$).

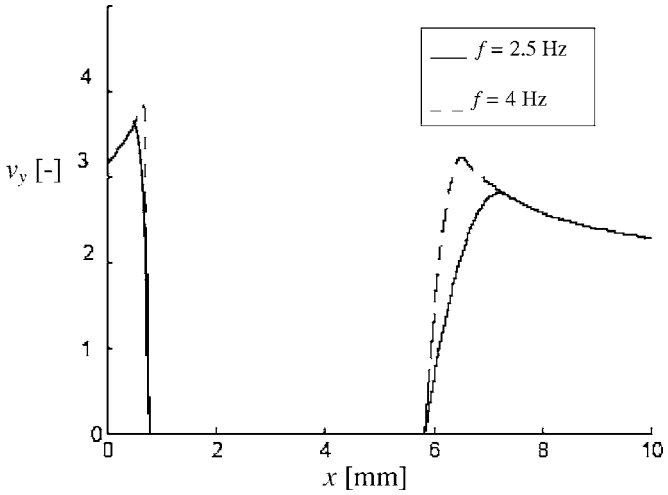

FIG. 6. Velocity v_y (normalized to u_0) along the line $y=0$, for the two cylinder geometry with $R=2.47$ mm and $d=1.56$ mm, at $f=2.5$ Hz and $f=4$ Hz, according to Eqs. (29) and (34).

In the two-dimensional problem of fluid flow around two circle-cylinders, the situation becomes more complicated, but the fluid flow can still be approximated by a composition of elementary plane flows. A suitable, equivalent, approach is to write a proper superposition of uniform and dipole solutions. As mentioned, the potential flow about a single cylinder in a uniform flow field is composed of the basic expressions for a parallel flow and for a dipole of given strength. To describe the nonviscous flow around multiple circular cylinders, the so-called method of images of Milne-Thomson for circle-cylinders can be utilized. With this method the boundary condition on the surface of the circle-cylinders can be satisfied to an arbitrary order of approximation.[23] Returning now to our solution, we can also recognize in Eq. (30) these components. Obviously, the term—x represents the uniform flow. Investigating the second term of this expression in the limit for large $z = x + iy$, we can see that it behaves as a sum of dipole solutions.

In the other limit, when the frequency parameter $\mu \to 1$, viscous effects will dominate. The presented matching solutions approach remains valid as long as μ is large, so that the boundary layer $\delta \sim R\mu^{-1/2}$ is small compared to the other dimensions, the cylinder radius and the mutual cylinder distance d. If δ becomes of the order of d, the boundary layer extends over all spacing between the cylinders of the probe and the used method does not apply. In that case, the two cylinders reduce to one object for acoustic waves imposed on the probe.

E. Consequences of the model

From the obtained expression for the stream function in the boundary layer and in the intermediate region, Eqs. (29) and (34), the velocity v_y can be calculated. We are particularly interested in its value along the line $y=0$.

This velocity, both in the intermediate region and in the thin boundary layers, is depicted in Fig. 6. It was calculated for the two cylinder geometry with a radius $R_0 = 2.47$ mm and a spacing of $d_0 = 1.56$ mm, and two values of the parameter μ, corresponding to $f=2.5$ Hz and $f=4$ Hz. For even

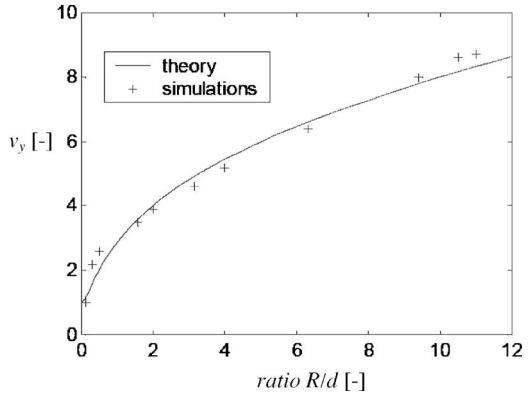

FIG. 7. Normalized velocity v_y at the central point $(x,y)=(0,0)$ as a function of the ratio R/d, according to theory and numerical simulations on the probe geometry with $\mu=10$.

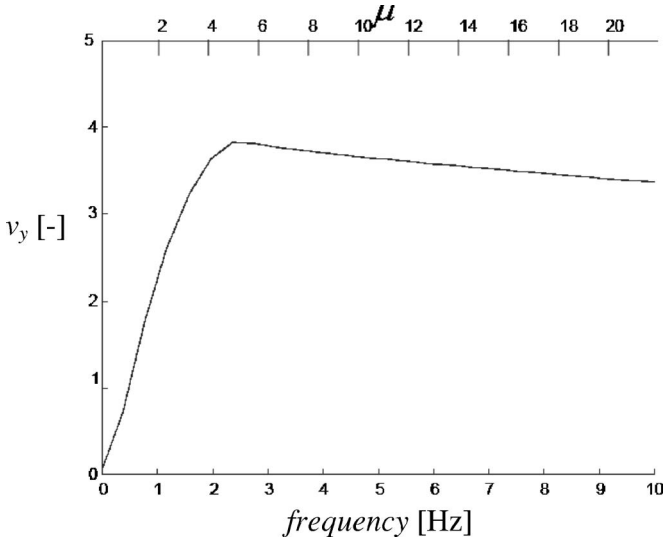

FIG. 8. Dependence of v_y on frequency, at the point where the sensor is located between the cylinders, $(x,y)=(500\ \mu\text{m},0)$. Calculated according to Eqs. (29) and (34).

lower frequencies, the boundary layer thickness is in the order of the mutual cylinder spacing and the approach leading to Eq. (34) is no longer valid. Let us now focus on the magnitude of the y velocity at the location of the particle velocity sensor, i.e., at the point $(x,y)=(0,0)$. In particular we will investigate the velocity in relation to the ratio of the cylinder radius and the spacing between the cylinders. With the coordinate transformation of Eq. (10) the mutual distance d between the cylinders, see Fig. 4, can be expressed as (with $a=1$):

$$d=\frac{2\sinh\eta_1}{\cosh\eta_1+1} \tag{39}$$

while the cylinder radius was $R=1/\sinh\eta_1$. The ratio R/d is therefore

$$\frac{R}{d}=\frac{1}{2(\cosh\eta_1-1)}. \tag{40}$$

From Eq. (29) and applying Eq. (11) we can determine the velocity v_y at $(x,y)=(0,0)$, where $(\xi,\eta)=(\pi,0)$. In Fig. 7 the dependence of $v_y(0,0)$ on the ratio R/d according to Eq. (29) is plotted. Also shown are numerical results from simulations on the real geometry of the probe with varying R/d, as will be discussed in more detail in Sec. III, rescaled to a constant value of the normalized frequency parameter μ to take into account the boundary layer effects. The value of this parameter, defined as $\mu=2\pi fl^2/\upsilon$, where for the characteristic dimension l was chosen the mutual cylinder distance d, was kept at a constant value of $\mu=10$. It must be mentioned that the theoretical curve is only valid as long as the probe dimensions, d and R, remain small with respect to the acoustic wavelength: R, $d\ll\lambda$.

In Fig. 8 the velocity is depicted as a function of frequency. The graph shows the dependence of the velocity on the normalized frequency parameter μ (upper axis) as well, indicating that the theory yields a characteristic frequency of about $\mu_c=4$. For $\mu>\mu_c$, the magnification remains almost constant.

The fact that high frequencies are amplified by a factor that does not depend much on frequency in the frequency range of our main interest, 50–1000 Hz, and that low frequency signals are attenuated due to the viscous effects, is of great importance for measurement applications. Low frequency signals, ubiquitous for this sensor,[24] should be suppressed while signals above a certain frequency are to be amplified. The package thus significantly contributes to the low-frequency roll off below about 10 Hz, which can be realized electronically also (actually most commercial probes have such an electronic high-pass filter).

III. COMPUTATIONAL FLUID DYNAMICS

A. The setup

To verify the validity of the theoretical analysis and the correctness of the used assumptions, we performed numerical simulations on two parallel cylinders immersed in a compressible flow, with the small particle velocity sensor in between, at a sensor temperature of 700 K.

For the numerical calculations on these structures we used CFDRC, a commercially available software program for fluid dynamical simulations.[25,26] The software provides a variety of tools for the simulation and analysis of fluid flow. In our approach for the numerical simulation of the fluid behavior around the sensor, three successive steps are to be distinguished. First, the volume of interest (the solution space) was divided into discrete control volumes or cells. Second, the boundary conditions, the initial conditions, and the equations to be solved at each cell were defined, as well as the numerical technique to solve the equations. And finally, after the solution, we extracted the needed information from the large amount of data generated in the solution process.

The solution space was defined as a system of two infinitely long cylinders of $R_0=2.47$ mm diameter at an ambient temperature of 300 K, with a small rectangular element of $0.2\times0.2\times2$ mm, representing a heated particle velocity sensor, of a fixed temperature of 700 K in between. The infiniteness of the cylinders was realized by imposing periodic boundary conditions on the flow. The fluid space around the probe was meshed using a structured grid of tetrahedral and

prismatic volume elements. The number of cells amounted to about 50 000; in the middle, around the sensor, the cells were made very dense. See Fig. 3(a).

Additionally, a solution space was defined with respect to the commercially available PU probe as shown in Fig. 2, the probe that was one of the motivations for this numerical analysis. This geometry consisted of a cylinder of approximately 8 cm radius and 15 cm height, in which the probe was positioned. This solution space comprised about 70 000 cells, with a dense grid in the middle around the sensor. See Fig. 3(b).

As a boundary condition, a plane propagating wave was imposed on the boundary of the large outer cylinder. This wave was described by a varying fluid particle velocity of magnitude u_0 and frequency f: $u(y,t)=u_0\cos(2\pi ft-ky)$, with k the wave number in the propagation direction y. The Navier-Stokes equations were solved at each fluid space element, together with the no-slip boundary condition on the probe surface and the assumption of a fully adiabatic process. The calculations were performed with a convergence criterion of 10^{-4}, using the SIMPLEC solution method, coupled with the ideal gas law.[25]

Besides, a constant ambient temperature and constant dynamic viscosity of, respectively, T=300 K and $\nu=1.5895\times10^{-5}$ m^2/s were assumed, an equilibrium fluid density of $\rho=1.1614$ kg/m^3, and an equilibrium pressure of $p_0=1.0\times10^5$ Pa in the fluid around the probe. It must be mentioned that both the presence of the particle velocity sensor and the temperature effects of this sensor, that causes a local temperature increase of the fluid due to the heated wires, have not been taken into account in the simulations on the probe geometry as depicted in Fig. 3(b). It was shown before[8,10] that the temperature effect of the wires is very localized since the temperature decreases to ambient values over a distance on the order of 100 μm. It is therefore presumable that this will only slightly influence the fluid flow around the heaters. As will be described in the next section, comparative simulations on the two infinite cylinders geometry show this assumption to be reasonable.

B. Simulation results

In the different simulations, the frequency f was varied between 0 and 10 kHz, and the magnitude u_0 was chosen as $3\times10^{-5}<u_0<1\times10^{-2}$ m/s (these values correspond in free space to sound levels of, respectively, 56 and 106 dB). Each simulation result provided the magnitude and phase of the particle velocity and the pressure at each point in space, such that the streamline pattern in the fluid could also be investigated. It was observed in the simulations that for the region of interest, $3\times10^{-5}<u_0<1\times10^{-2}$ m/s, all dynamics were linear in u_0, i.e., an increase of the amplitude of the imposed acoustic wave led to an equal increase of the velocities and pressures at all points in space.

For the two infinite cylinders geometry, we investigated first the influence of the presence of the small rectangular obstacle and of its temperature on the flow profile and on the magnitude of the particle velocity in between the cylinders.

The spacing between the cylinders was equal to 1.1 mm.

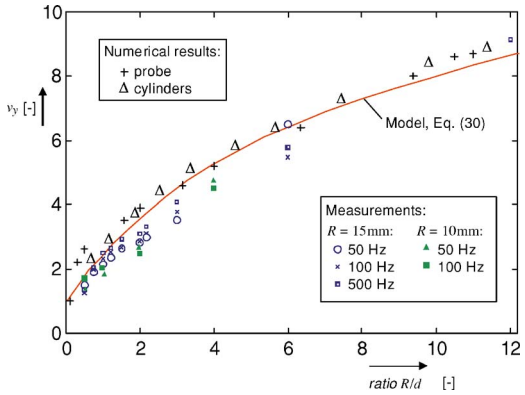

FIG. 9. (Color online) Particle velocity v_y at the point in the center between the two cylinders $[(x,y)=(0,0)]$, normalized by the imposed particle velocity at infinity, measured at different frequencies, with the sensor between two cylindrical objects. For comparison, the results of the computational analysis are shown, both on the commercial probe and on two infinite cylinders. For an air viscosity of $\nu=1.5895\times10^{-5}$ m^2/s, the theoretical curve following from Eq. (30) is also depicted, represented by the drawn line. The experimental results at 50 Hz were obtained by means of the shaker setup and therefore had to be scaled by a factor of 1.35 as described in Sec. IV; for 100 and 500 Hz the loudspeaker was used. Different cylinder radii (R =10 mm and R=15 mm) were investigated.

This spacing d corresponds to the effective distance between the cylinders of the commercial probe, which is the mutual cylinder spacing of 1.56 mm minus the thickness of the thin strip (a printed circuit board) on which the sensor is mounted (see Fig. 2).

When the temperature of the rectangular element was set to be T=700 K, a magnification of the particle velocity between the cylinders (with respect to the applied particle velocity u_0 of the incident sound wave) of 3.6±0.1 was found; when its temperature was the same as the ambient temperature, T=300 K, the amplification was 3.4±0.1. Apparently, the higher temperature results in only a slight increase of the particle velocity. The rectangular element itself had, taking into account the numerical error of the calculations, only a small influence on the magnitude of the particle velocity at the central point between the cylinders (3.5±0.1 and 3.4±0.1 for the situations with and without the element, respectively).

Next, the dimensions of the cylinders were varied. Keeping the mutual cylinder spacing d at a constant value of 1.1 mm, the cylinder radius R was varied in small steps from 1.1 to 12 mm. The same radii were also investigated at a mutual spacing of d=2.2 mm. The result of this, the magnification, i.e., the normalized particle velocity in between the cylinders, as a function of R/d is shown in Fig. 9. Also shown are the theoretical dependence on the ratio R/d, and measurement results described in Sec. IV.

The above-mentioned results show that both the effect of the sensor temperature and the effect of the presence of a small obstacle in the flow are relatively small. The following simulations, on the factual probe of specific interest, were therefore performed at constant temperature and without a representation of the sensor element, which reduced considerably the duration of the computations.

With respect to this specific geometry, we defined a number of points located in and around the probe to consider in particular. Point A is located in between the two small

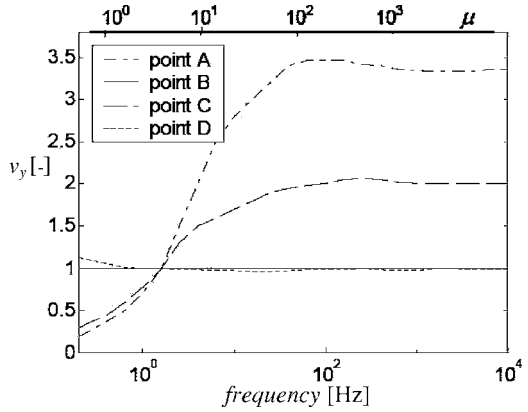

FIG. 10. Amplitude of the particle velocity at different points in and around the probe, normalized to the magnitude u_0 of the incoming wave. The upper horizontal axis shows the dimensionless frequency $\mu=2\pi fl^2/\nu$.

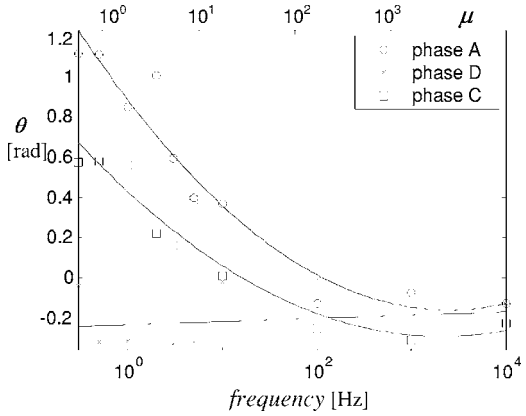

FIG. 11. Phase shift of the signals at points A, C, and D with respect to the phase at these points due to the imposed wave when there is no probe (i.e., the phase shift of A, C, and D due to the presence of the probe), as a function of frequency and μ. The lines are polynomial fits only to show the trends of the curves, they are not based on a model.

cylinders (where the sensor is placed in reality, but not in the simulation), point B is at a distance of 8 cm in front of the probe (on the outer boundary where the acoustic wave is imposed), C is located at 6.5 mm left from the center, and D was defined at 3 cm above A to investigate the phase behavior of the wave. See Fig. 3(b).

When the frequency rises, the particle velocity (normalized to the value u_0 of the imposed wave) increases at both points A and C, as shown in Fig. 10. One sees that, especially at A, a large amplification of the particle velocity is attained. This magnification approaches a value of about 3.3 at a frequency of 50 Hz. For frequencies below 1 Hz, however, the normalized particle velocity at A is smaller than 1, and decreases to 0.2 at 0.5 Hz. The same tendency is observed at C, a representative point for the region just next to the probe. The normalized signal increases from 0.3 at 0.5 Hz up to 1.7 at 10 Hz and remains almost constant above 100 Hz. With the perceived frequency behavior it seems natural to define a characteristic frequency to characterize the properties of this probe. Noting that at approximately $f=1.5$ Hz both points A and C have a velocity amplification of 1, a reasonable choice seems to define this characteristic frequency of about $f_c=1.5$ Hz, so that for frequencies below f_c, the (scaled) particle velocity amplitudes at A and C are lower than one, whereas for $f>f_c$, they increase.

The time dependence of the particle velocities at the points of most interest, A, C, and D, was analyzed in order to determine the local phase shift due to the presence of the probe (the difference between the phase of those points and the phase of those points if there were no probe at all, i.e., if the wave propagated in free space). Figure 11 shows this phase shift θ of A, C, and D, defined as $\theta_A=\phi_A-\phi_{A,\text{without any probe}}$. For high frequencies, θ_A and θ_C approach 0, while θ_D is, within the error margins, almost frequency independent and constant at -0.1 ± 0.1 rad. The curves in Fig. 11 are polynomial fits on the logarithmic frequency scale and are only depicted to show the trends of the curves.

In Sec. II it was mentioned the problem can be made nondimensional by scaling to a dimensionless frequency μ,

$$\mu=\frac{2\pi fl^2}{\nu}, \tag{41}$$

where l is a characteristic length of the geometry, for which we take the radius of the two small cylinders, and ν the kinematic viscosity of the fluid. In the original situation of the specific probe in air, we have $\nu_0=1.5895\times10^{-5}$ m$^2/s$ and $l=R_0=2.47$ mm. Simulations were performed for different viscosities, varying in an extended range of $0<\nu<10\nu_0$, the case $\nu_0=0$ corresponding to a completely nonviscous gas. The probe itself was also scaled (with all dimensions scaling proportionally to l) in the range $R_0/2<l<10R_0$. It was found that, indeed, the relevant independent parameter for the problem is the scaled frequency μ. Further we verified that the simulated velocity values at all points in space were linear in u_0, the magnitude of the incoming sound wave, for values $u_0<10^{-2}$ m/s. The dependence of the particle velocity at the different points as a function of the dimensionless parameter μ is seen in Fig. 10. The velocity has been normalized by dividing through the velocity amplitude u_0 of the incoming wave at the boundary.

According to Fig. 10 it was noted that two different frequency regimes can be distinguished in which the flow profile is essentially different. For frequencies well below 1.5 Hz, the signal at A is strongly attenuated. Since the boundary layer thickness δ is in the order of $\delta\sim\sqrt{\nu/2\pi f}$, one finds that at 1 Hz, this layer is approximately equal to the mutual cylinder spacing. Therefore, point A is then situated in a large viscous boundary layer that extends over all space between the two cylinders. For frequencies much higher than 1.5 Hz, viscous effects become less and less important, the boundary layer thickness decreases, and the gas flows at A with increased particle velocity. Figure 12 is a visualization of this phenomenon that the particle velocity between the cylinders is attenuated for low frequencies and amplified for higher frequencies. For low frequencies ($f\sim1$ Hz) the fluid tends to flow around the probe as a whole while the velocity in the boundary layer is low, as is seen in Fig. 12(a). This effect disappears for high frequencies.

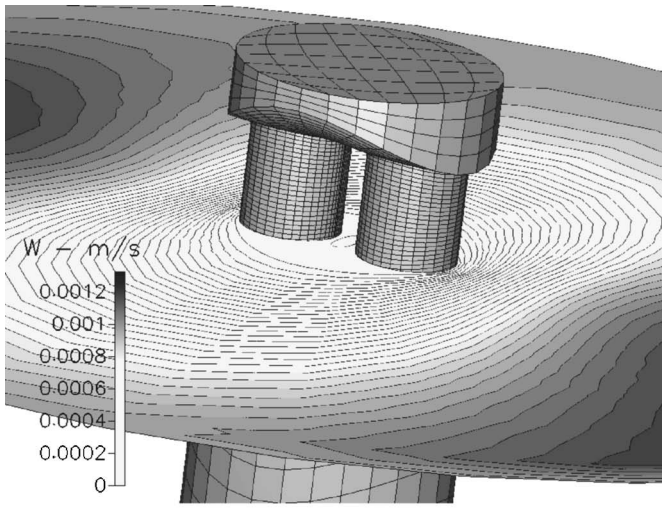

(a)

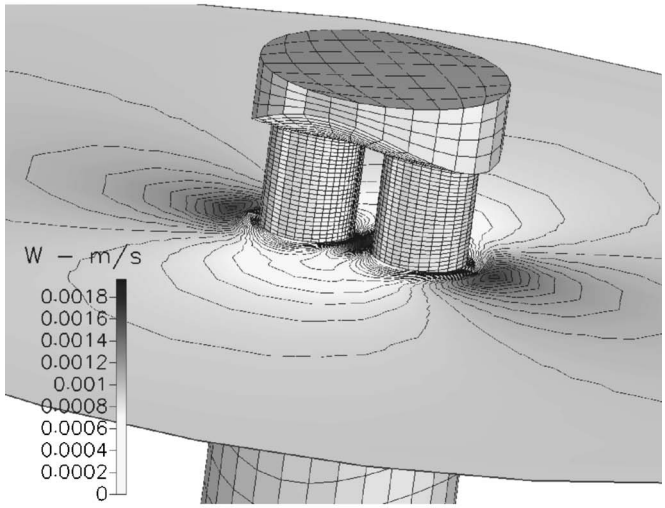

(b)

FIG. 12. (a) Contour plot of the particle velocity in a horizontal plane, for $f=0$ Hz. ($v_0=1$ mm/s). (b) As in (a) for $f=10$ Hz ($v_0=1$ mm/s).

The two different regimes can be distinguished also in terms of a characteristic value of the parameter μ, giving $\mu<\mu_c$ and $\mu>\mu_c$ with $\mu_c\approx 3.5$.

Next, we analyzed the dependence of the velocity amplification at A for high frequencies on the probe geometry. The dimensions of the two cylinders and their mutual distance were varied, with the mutual spacing between the cylinders d varying in the range $d_0/10<d<3d_0$ and the cylinder radius R changing from $R_0/2<R<10R_0$. The value R_0, the cylinder radius of the actual probe, was equal to 2.47 mm; for d_0 we took the effective gap distance between the cylinders, $d_0=1.1$ mm, corresponding to the mutual cylinder spacing minus the thickness of the strip the sensor is mounted on. Figure 13 shows this dependence of the normalized velocity at the central point between the cylinders, A, as a function of R/d, at a frequency of 10 Hz.

IV. EXPERIMENTAL WORK

To determine the effects of two cylindrical pillars on the output signal of the particle velocity sensor, a setup was realized to compare two identical particle velocity sensors. One sensor had no adjacent cylinders and was used as a reference, while the other sensor was placed between two small cylindrical pillars of varying diameter. The setup consisted of two movable pillars of 5 cm height and diameters of 20 and 30 mm, allowing for a variation of the mutual pillar distance d. A second separate particle velocity sensor without adjacent cylinders was used as a reference sensor and placed at a relatively large distance, about 10 cm, from the pillars. A photograph of the measurement setup is shown in Fig. 14(a). The sound signal was generated by a loudspeaker acting as a point source that was placed at a distance of 0.5 m from the setup. The distance between the reference sensor and the cylinders pair should be as large as possible to avoid effects of this construction on the output signal like acoustic reflections. On the other hand, the sound field due to the sound source must be as similar as possible for both sensors. An acceptable compromise between these requirements was found at a distance between the sensors of 10 cm.

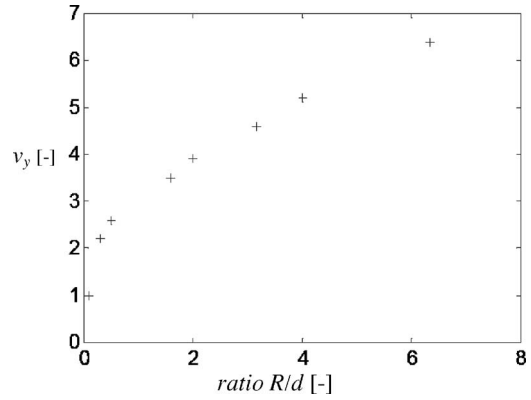

FIG. 13. Normalized particle velocity v at point A, as a function of R/d, according to the computational analysis, with $f=10$ Hz and $\nu=1.5895\times10^{-5}$ m^2/s.

We performed a reference measurement without the two pillars mounted to determine the transfer function between the particle velocity sensor of investigation and the reference sensor. This transfer function had a value close to 10 in a frequency range of 100 Hz–1.5 kHz, indicating that in this frequency band no irregular effects occur. By varying the distance d between the pillars and the radius R of the pillars, the transfer function, i.e., the ratio of the output signal of the sensor and the reference sensor, was determined for a wide range of R/d values. The division by the reference measurement permitted one to eliminate any differences in the responses of the sensors so that merely the effects of the cylindrical obstructions were measured. Results of these measurements, in a frequency range of $100<f<1500$ Hz, are plotted in Fig. 14(b).

For the low-frequency response use was made of a "shaker" setup, providing a white noise excitation from 10 to 500 Hz. The movement of the sensor due to the shaker setup is assumed to yield a sensor output analogous to that due to a particle velocity of a sound wave. Similar to that described earlier, the cylinders pair with the central sensor, and a reference sensor, were mounted on the shaker and the transfer function was determined for varying R/d ratios. Not

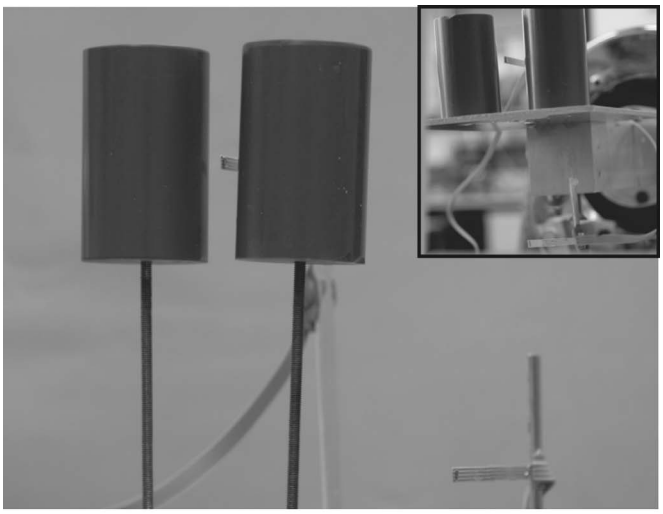

(a)

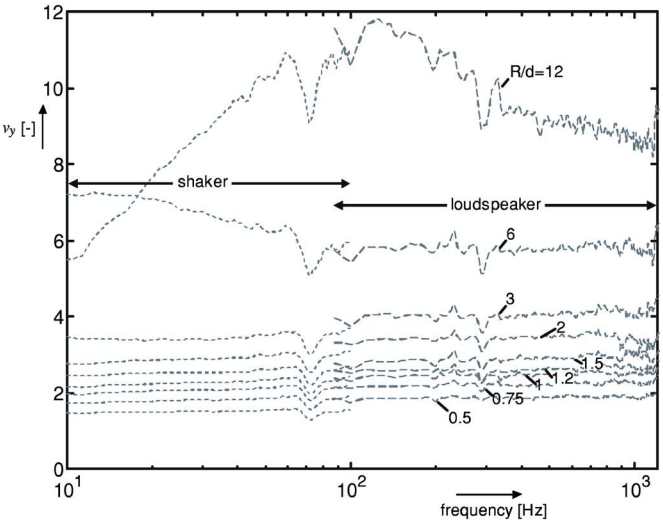

(b)

FIG. 14. (Color online) (a) Photograph of the experimental setup, showing the particle velocity sensor between the two small cylinders and the reference senor, mounted on a tripod. The inset shows the two cylinders mounted on the shaker platform. (b) Normalized velocity v_y in the center between the two cylinders [at $(x,y)=(0,0)$], as a function of frequency, with the ratio R/d as a parameter. For frequencies below 100 Hz, the measurements were performed by means of the "shaker" setup (with $R=15$ mm); for the higher frequencies a loudspeaker was used. Both sets of measurements are depicted by different symbols. The shaker measurements were all scaled by a factor of 1.35 to match optimally with the loudspeaker results for the higher frequencies.

only the mutual distance d was varied, also different cylinder dimensions ($R=10$ mm and $R=15$ mm) were investigated for this purpose. Although this experiment produced useful data for frequencies up to 500 Hz, the results for frequencies between 10 and 150 Hz were used.

The results for different frequencies were already shown in Fig. 9. As one can see in Fig. 9, for the frequencies $f=50$ Hz and $f=100$ Hz, the experimentally determined velocities lie somewhat below the simulation and theoretic results for ratios R/d around approximately 3. A possible explanation may be found in the fact that at relatively large cylinder spacings, the horizontal and vertical dimensions of the total object (two cylinders and their gap in between) are on the same order of magnitude: The height h is not large anymore with respect to the other dimensions. This may lead to a flow over the structure as a whole, the gas tends to stream over what is perceived as a single obstacle. This may result in a decrease of the measured velocity at the sensor location.

For the current probe geometry of Fig. 2, i.e., the two sensor wires in between two cylinders of 4.94 mm diameter and an effective gap of 1.1 mm, yielding $R/d=2.2$, the amplification (this is the ratio of the output signal with / without probe package) was found to be 3.2 at 500 Hz. It must be noted that the precise value of this amplification is strongly dependent on the specific mounting of the particular probe under investigation.

Figure 14(b) illustrates the measurement results of the shaker setup, using pillars with a radius of $R=15$ mm, and the measurements by means of the loudspeaker together, as a function of frequency with R/d as a parameter. In the overlapping frequency range $85<f<100$ Hz the shaker and the loudspeaker results are plotted conjointly. The shaker measurements as they are depicted in Fig. 14(b) were scaled by a factor of 1.35 to correspond optimally to those of the loudspeaker. This division by 1.35 (the same factor for all shaker measurements) was required to match the two measurement series in the adjoining frequency ranges: ideally this scale factor is unity. Although the emergence of a difference between the shaker generated signal and that of the loudspeaker is not fully unexpected, the origin of this scale factor is not completely understood yet and is an important point of further investigation.

The dip at a frequency of about 70 Hz is attributed to a mechanical resonance of the shaker setup; it shows a frequency shift if the shaking platform is placed vertically instead of horizontally. For frequencies above 50 Hz the amplification is nearly independent of frequency for R/d ratios up to 12. At $R/d=12$ the low frequency "cut off" effect is manifest: A cut off frequency of approximately 50 Hz is observed. With $f=50$ Hz and $l\approx 0.5$ mm, we find then for the dimensionless characteristic frequency, $\mu_c=2\pi fl^2/\nu\approx 5$, which is close to the theoretical value of $\mu_c\approx 4$.

V. CONCLUSIONS

We have analyzed the effects of two cylindrical objects adjacent to an acoustic sensor on the velocity profile around the sensor. This was done by a theoretical analysis on two parallel infinite cylinders, together with numerical simulations on the geometry. The theoretical two-dimensional analysis provided an analytical expression for the stream function around the cylinders. The supplemental computational simulations showed that both the presence of the small particle velocity sensor between the two cylinders and its high local temperature have only a small effect on the flow profile in and around the cylinders and on the particle velocity near the sensor. A large magnification of the particle velocity in between the cylinders for frequencies above 4 Hz was found in these simulations.

As a specific example of the two cylinder geometry, a commercially available probe was investigated experimen-

tally and by means of a computational analysis on this geometry. The magnification in this probe was found to increase up to approximately 3 in a frequency range from 50 up to 1000 Hz, being 3.2 at 500 Hz.

Although in these simulations the geometry differed from the ideal two-dimensional case of two cylinders, both the theory and the simulations on two cylinders are seen to give an adequate description for the fluid flow in the package of the probe. Therefore, with the two-dimensional model the so-called "package gain" at high frequencies can be described. For low frequencies, viscous effects dominate and signals are attenuated. This is important for acoustic measurement applications, in which low frequency signals should be suppressed and higher frequencies be amplified. In this respect one can define a characteristic value μ_c, of the dimensionless frequency $\mu = 2\pi f l^2/\nu$, below which frequency acoustic signals are attenuated and above which they are amplified. Experimental results show an estimated value of $\mu_c \approx 5$, theory yields $\mu_c \approx 4$ where simulations give $\mu_c \approx 3.5$; a satisfactory agreement.

We found a relatively good correspondence among simulations, theory, and experiments. The two-dimensional analysis has provided a better understanding of the gas flow for low Reynolds numbers around parallel cylinders and since it is seen to be partly applicable for the specific probe too it opens the way, together with the numerical simulations, for further optimization of the probe geometry.

ACKNOWLEDGMENTS

The authors would like to thank the Dutch Technology Foundation STW for financial support. Additionally, we thank Professor Hoeijmakers for his fruitful comments.

[1]H. E. de Bree, P. J. Leussink, M. T. Korthorst, H. V. Jansen, T. S. J. Lammerink, and M. C. Elwenspoek, "The Microflown: A novel device measuring acoustical flows," Sens. Actuators, A **54**, 552–557 (1996).
[2]W. F. Druyvesteyn, H. E. de Bree, and M. Elwenspoek, *A New Acoustic Measurement Probe; The Microflown*, (IOA, London, 1999).
[3]H. Schurer, P. Annema, H. E. de Bree, C. H. Slump, and O. E. Herrmann, "Comparison of two methods for measurement of horn input impedance," Proceedings of the 100th AES convention, Copenhagen, 1996.
[4]F. J. M. van der Eerden, H. E. de Bree, and H. Tijdeman, "Experiments with a new acoustic particle velocity sensor in an impedance tube," Sens. Actuators, A **69**, 126–133 (1998).
[5]H. E. de Bree, T. Korthorst, P. J. Leussink, H. Jansen, and M. Elwenspoek, "A method to measure apparent acoustic pressure, flow gradient and acoustic intensity using two micromachined flow microphones," Eurosensors X, Leuven, 1996.
[6]H. E. de Bree, "Add-on Microflown for a high-end pressure gradient microphone," Proceedings of the 109th AES Convention, Los Angeles, 2000, No. 5181.
[7]H. E. de Bree, H. V. Jansen, T. S. J. Lammerink, G. J. M. Krijnen, and M. Elwenspoek, "Bi-directional fast flow sensor with a large dynamic range," J. Micromech. Microeng. **9**, 186–189 (1999).
[8]V. B. Svetovoy and I. A. Winter, "Model of the Microflown microphone," Sens. Actuators, A **86**, 171–181 (2000).
[9]J. W. van Honschoten, V. B. Svetovoy, G. J. M. Krijnen, and M. Elwenspoek, "Analytic model of a two-wire thermal sensor for flow and sound measurements," J. Micromech. Microeng. **14**, 1468–1477 (2004).
[10]J. W. van Honschoten, G. J. M. Krijnen, V. B. Svetovoy, H. E. de Bree, and M. Elwenspoek, "Optimisation of a two-wire thermal sensor for flow and sound measurements," Proc. MEMS 2001, Interlaken, Switzerland, pp. 523-526.
[11]Z. Carrière, "Double boundary layers in oscillatory viscous flow," J. Phys. Radium **10**, 673-677 (1929).
[12]E. N. Andrade, "On the circulations caused by vibrations of air in a tube," Proc. R. Soc. London, Ser. A **134**, 445-470 (1931).
[13]H. Schlichting, "Berechnung ebener periodischer Grenzschichtströmungen, (Calculation of periodical boundary layer flows)" Phys. Z. **23**, 327-335 (1932).
[14]N. Riley, "Oscillatory viscous flows," Mathematika **12**, 161-175 (1965).
[15]C. Y. Wang, "On high-frequency oscillatory flows," J. Fluid Mech. **32**, 55–68 (1968).
[16]Z. Zapryanov, Zh. Kozhoukharova, and A. Iordanova, "On the hydrodynamic interaction of two circular cylinders oscillating in a viscous fluid," J. Appl. Math. **39** 204-220 (1988).
[17]A. P. Zhuk, "A study of the interaction of an acoustic wave in a viscous liquid with two cylinders placed in parallel," Int. Appl. Mech. **27**, 321–327 (1991).
[18]R. Meneghini, F. Saltara, C. L. R. Siqueira, and J. A. Ferrari, "Numerical simulation of flow interference between two circular cylinders in tandem and side-by-side arrangements," J. Fluids Struct. **15**, 327–350 (2001).
[19]J. W. van Honschoten, D. R. Yntema, M. Dijkstra, V. B. Svetovoy, R. J. Wiegerink, and M. Elwenspoek, "Analysis of packaging effects on the performance of the microflown," Proceedings of the DTIP Conference of MEMS & MOEMS, Stresa, Italy, ISBN 2-916187-03-0, 2006.
[20]L. D. Landau and E. M. Lifschitz, *Fluid Mechanics*, Course of Theoretical Physics Vol. **6**, 2nd ed. (2003), Butterworth-Heinemann, Burlington, pp. 20-21.
[21]I. S. Gradshteyn and I. M. Ryzhik, *Table of Integrals, Series, and Products*, corrected and enlarged ed. (Academic, New York, 1980).
[22]R. W. Fox and A. T. McDonald, *Introduction to Fluid Mechanics*, 3rd ed. (John Wiley & Sons, New York, 1985).
[23]L. M. Milne-Thomson, *Theoretical Hydrodynamics* (Courier Dover, London, 1996).
[24]J. W. van Honschoten, W. F. Druyvesteyn, H. Kuipers, R. Raangs, and G. J. M. Krijnen, "Noise reduction in acoustic measurements with a particle velocity sensor by means of a cross-correlation technique," Acta. Acust. Acust. **90**, 394–355 (2004).
[25]CFD Research Corporation, "Technologies for engineering simulations," Huntsville, AL, www.cfdrc.com Accessed 4/9/2007.
[26]H. Versteeg and W. Malalasekra, *An Introduction to Computational Fluid Dynamics: The Finite Volume Method Approach* (Pearson Education Ltd., London, 1996).